Electronic Supplementary Material (ESI) for Nanoscale.

Supplementary Information

Tungsten nitride-coated graphene fibers for high-performance wearable supercapacitors

Ali Salman, Suchithra Padmajan Sasikala, In Ho Kim, Jun Tae Kim,

Gang San Lee, Jin Goo Kim and Sang Ouk Kim*

National Creative Research Initiative Center for Multi-Dimensional Directed Nanoscale Assembly, Department of Materials Science and Engineering, KAIST, 291 Daehak-ro, Yuseong-gu, Daejeon 34141, Republic of Korea.

*Corresponding author email: sangouk.kim@kaist.ac.kr

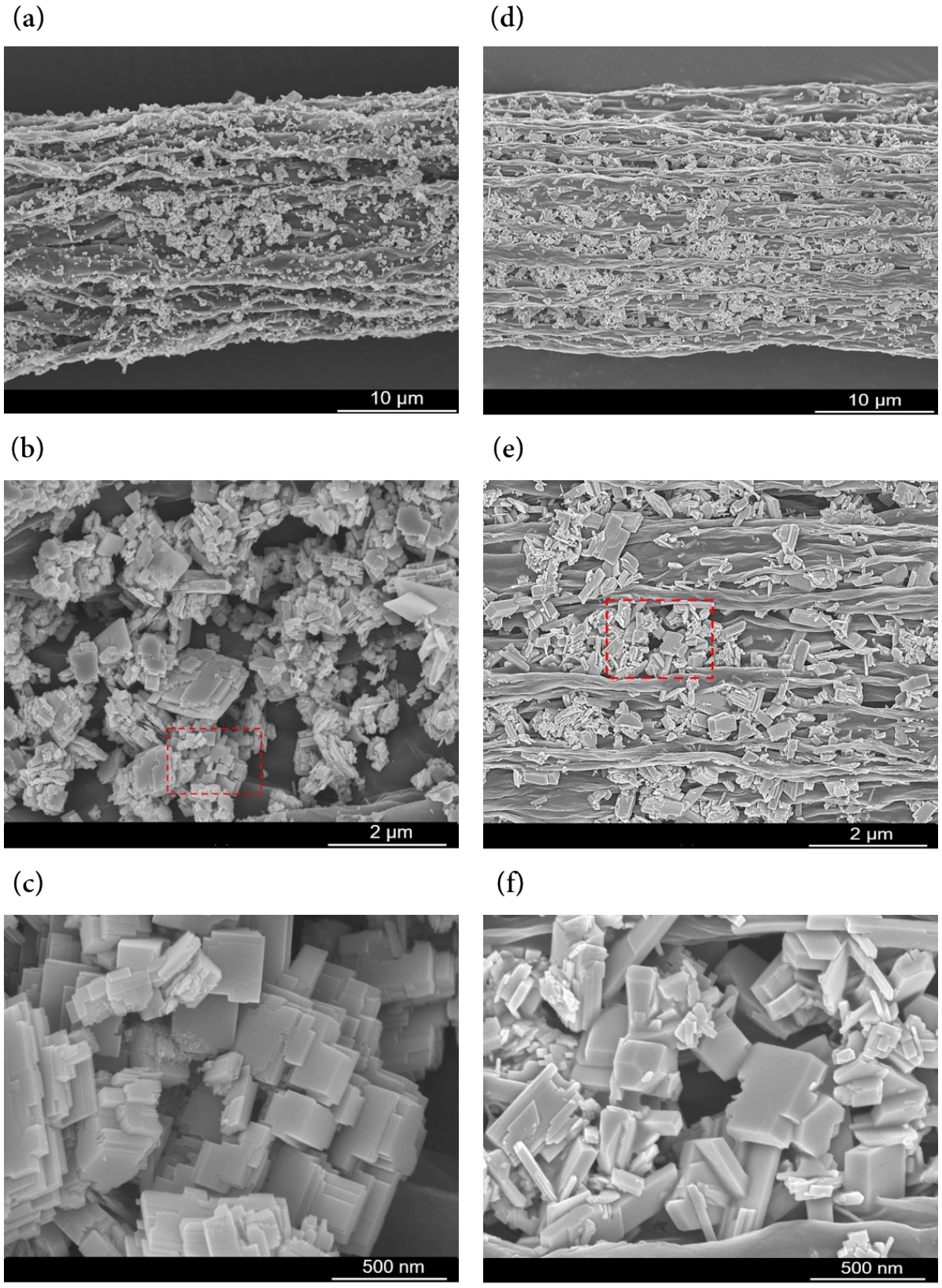

Figure S1. (a-c) Lateral SEM images of WO_3-GOF at increasing magnification. S1(c) shows the area depicted in S1(b) in red. (d-f) Lateral SEM images of WN-rGOF at increasing magnification. S1(f) shows the area depicted in S1(e) in red.

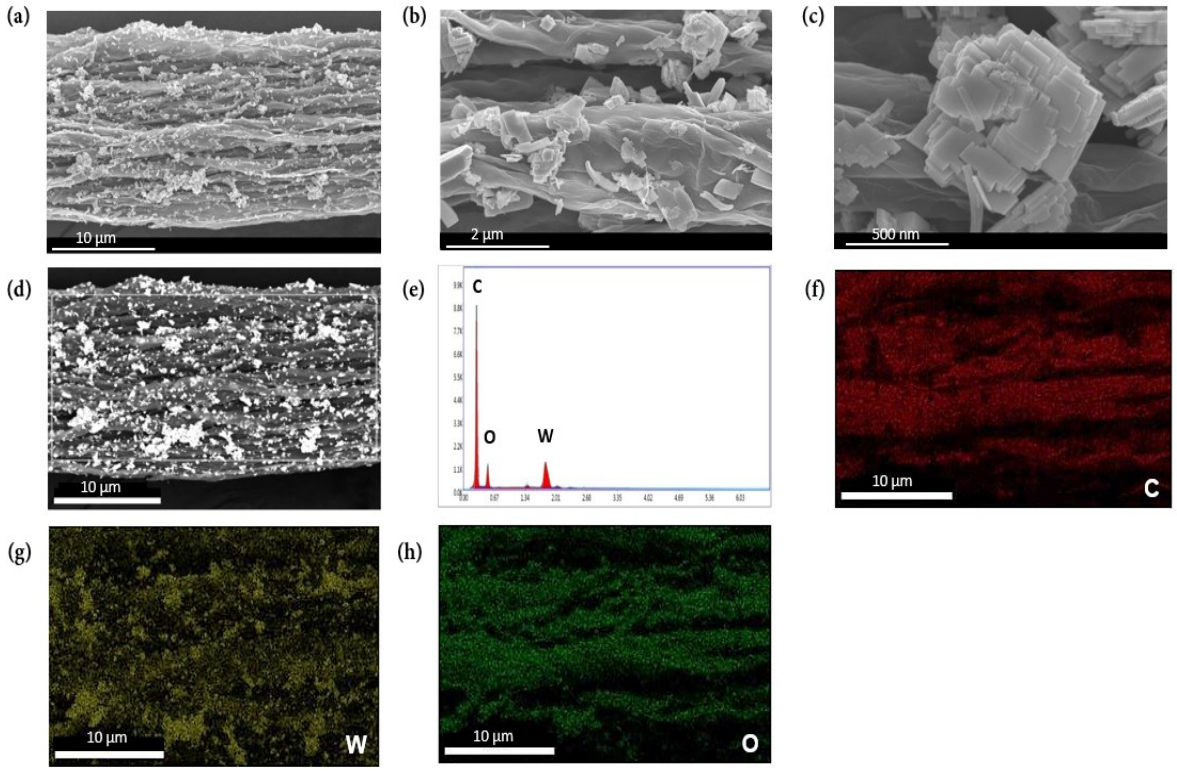

Figure S2. (a-c) Lateral SEM images of WO_3-rGOF with increasing magnification showing the WO_3 nanocubes attached to the fiber. (d) The corresponding back-scattered electron (BSE) image of WO_3-rGOF displaying the presence of the active material on the fiber surface. It also outlines the region of the fiber selected for EDS analysis. (e) The associated EDS Spectra of WO_3-rGOF. (f-h) EDS elemental maps of WO_3-rGOF.

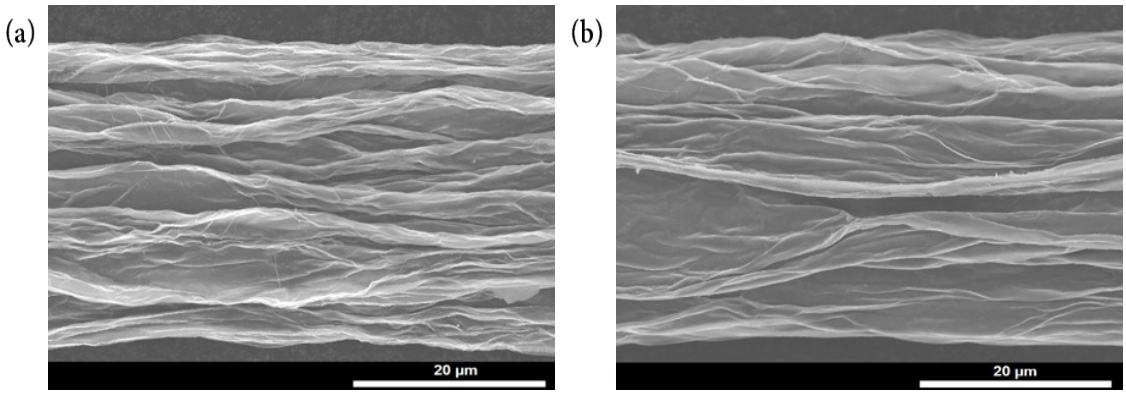

Figure S3. Lateral SEM images of (a) as-spun GO fiber and (b) rGO fiber.

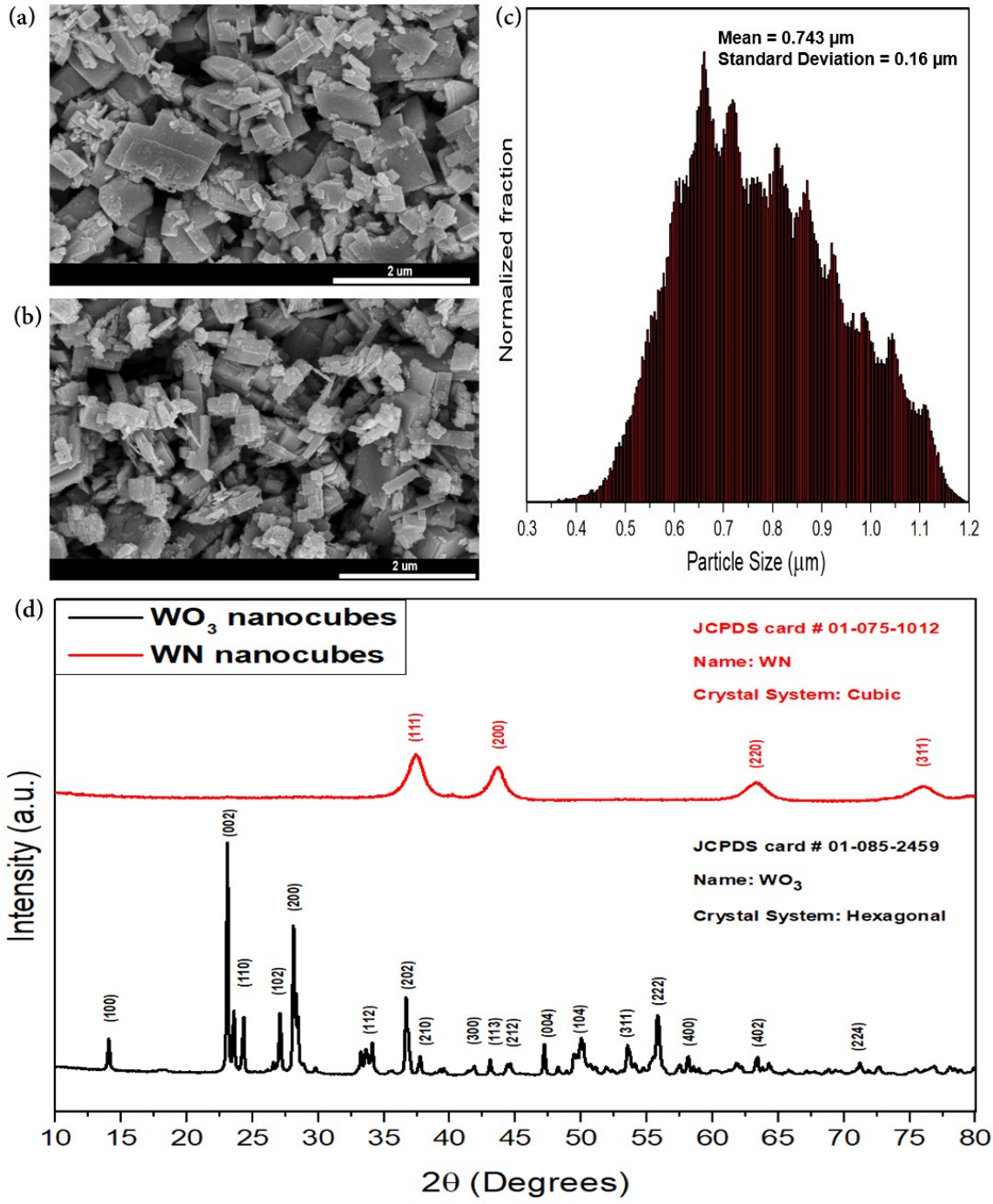

Figure S4. (a) SEM image of WO_3 nanocubes (synthesized at 180°C). (b) SEM image of WN nanocubes (synthesized at 700°C). (c) The corresponding particle size distribution of WN nanocubes. (d) XRD analysis results for WO_3 nanocubes and WN nanocubes.

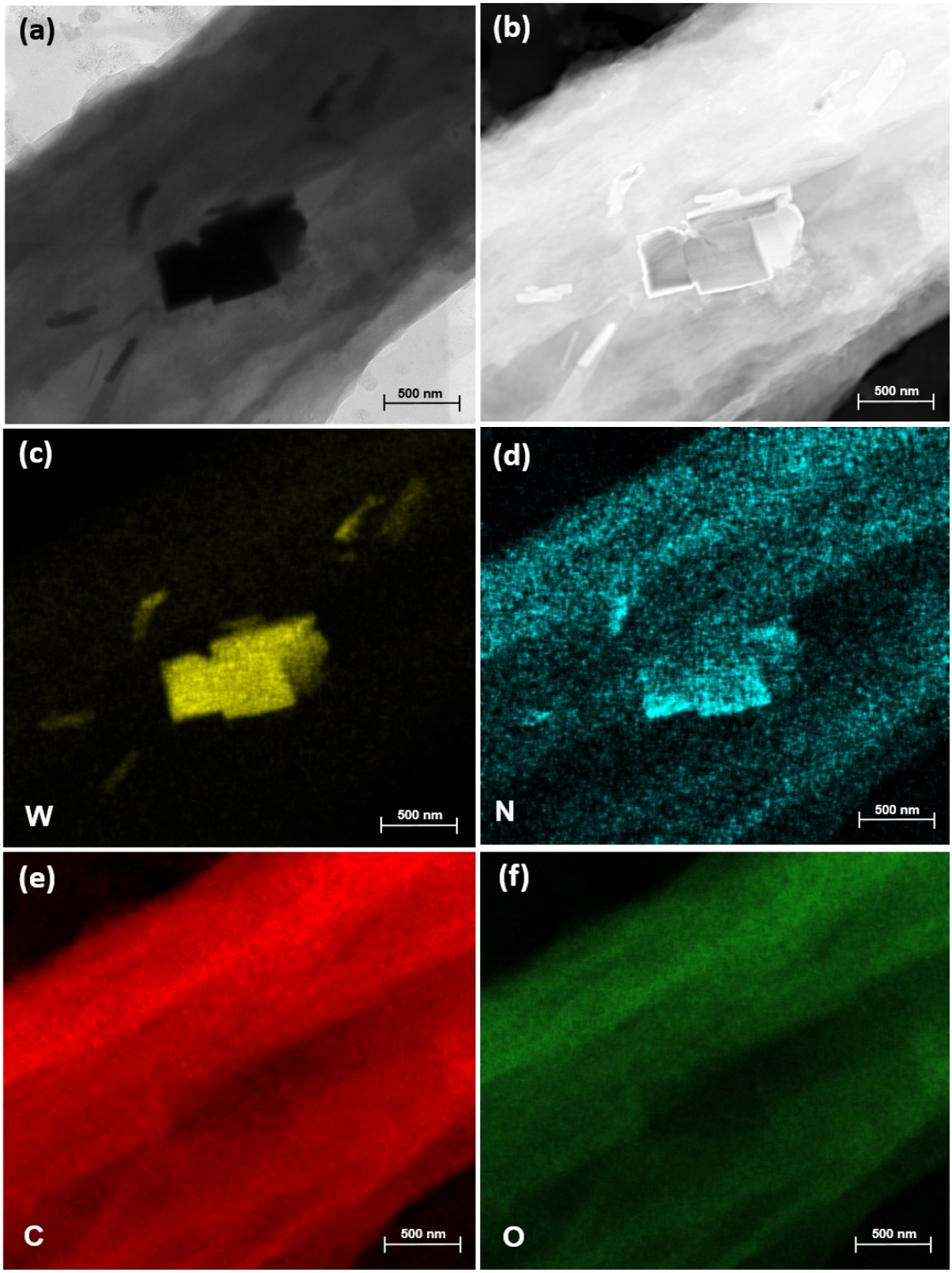

Figure S5. TEM, HAADF images and the corresponding EDS maps of WN-rGOF (a) TEM image of WN-rGOF (b) HAADF image of WN-rGOF (c) EDS map of W (d) EDS map of N (e) EDS map of C (f) EDS map of O.

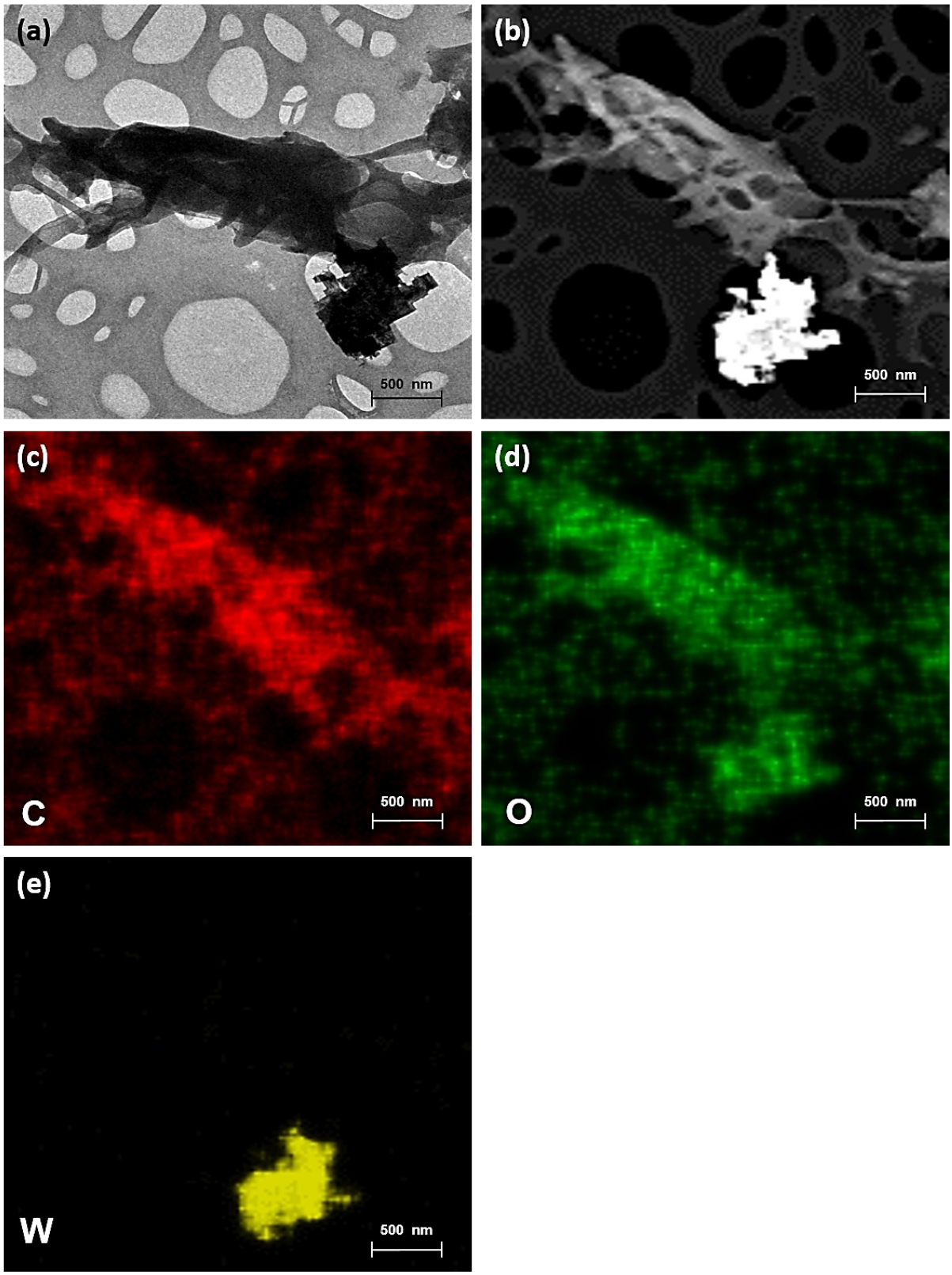

Figure S6. TEM, HAADF images and the corresponding EDS maps of WO_3-rGOF (a) TEM image of WO_3-rGOF (b) HAADF image of WO_3-rGOF (c) EDS map of C (d) EDS map of O (e) EDS map of W.

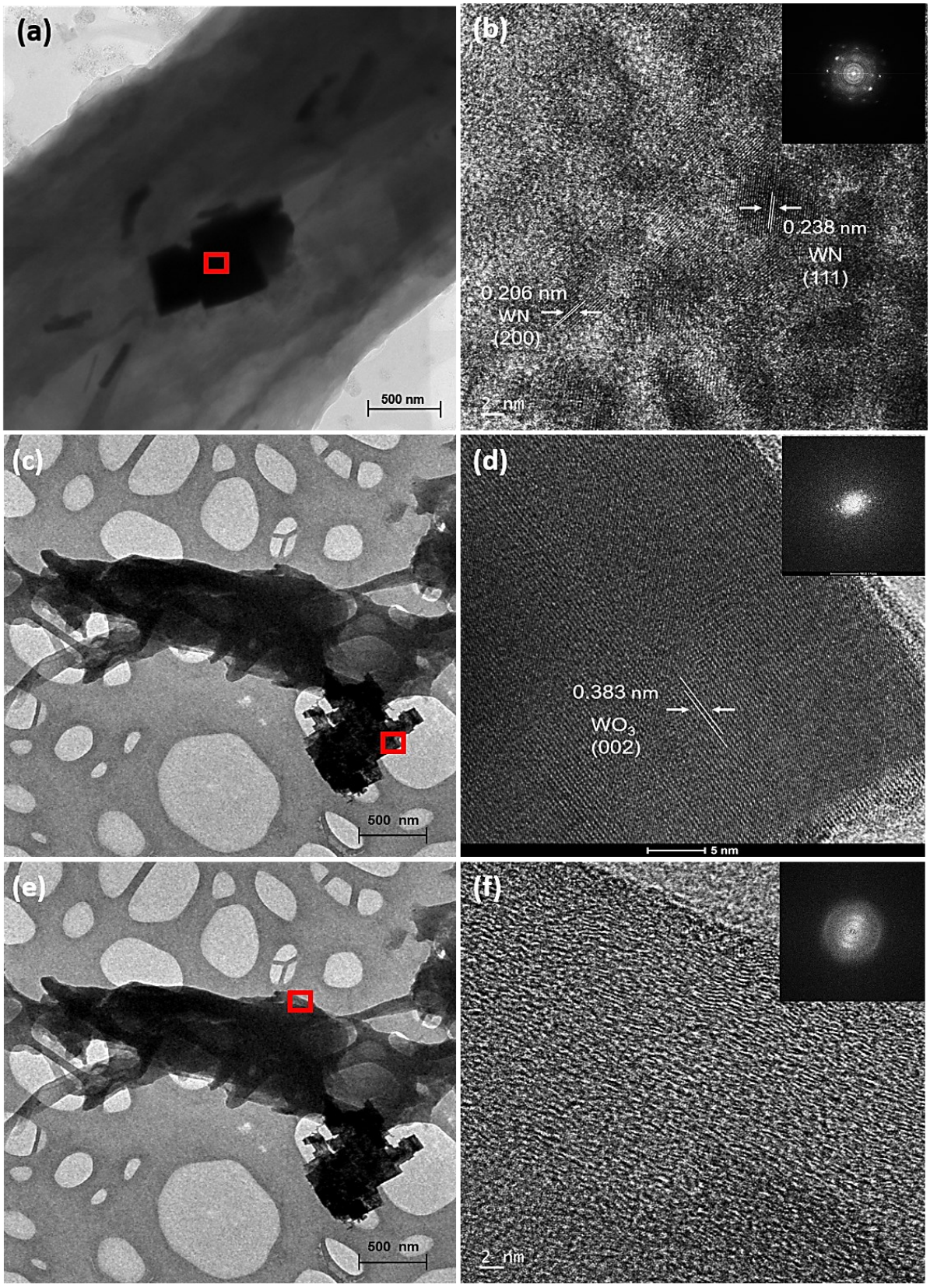

Figure S7. (a) TEM image of WN-rGOF (b) HRTEM image of WN nanocube attached with a portion of the fiber. Inset is the SAED pattern of the same area. (c) TEM image of WO_3-rGOF (d) HRTEM image of WO_3 nanocube attached with a portion of the fiber. Inset is the SAED pattern of the same area. (f) HRTEM and SAED of the localized fiber part of WO_3-rGOF shown in (e).

Element	rGOF XPS atomic ratios (%)	WO_3-rGOF XPS atomic ratios (%)	WN-rGOF XPS atomic ratios (%)
C	78.82	65.96	69.57
W		6.16	5.89
O	21.18	27.88	16.13
N			8.41

Table S1. Atomic ratios of elements in the fibers as determined through XPS survey scans.

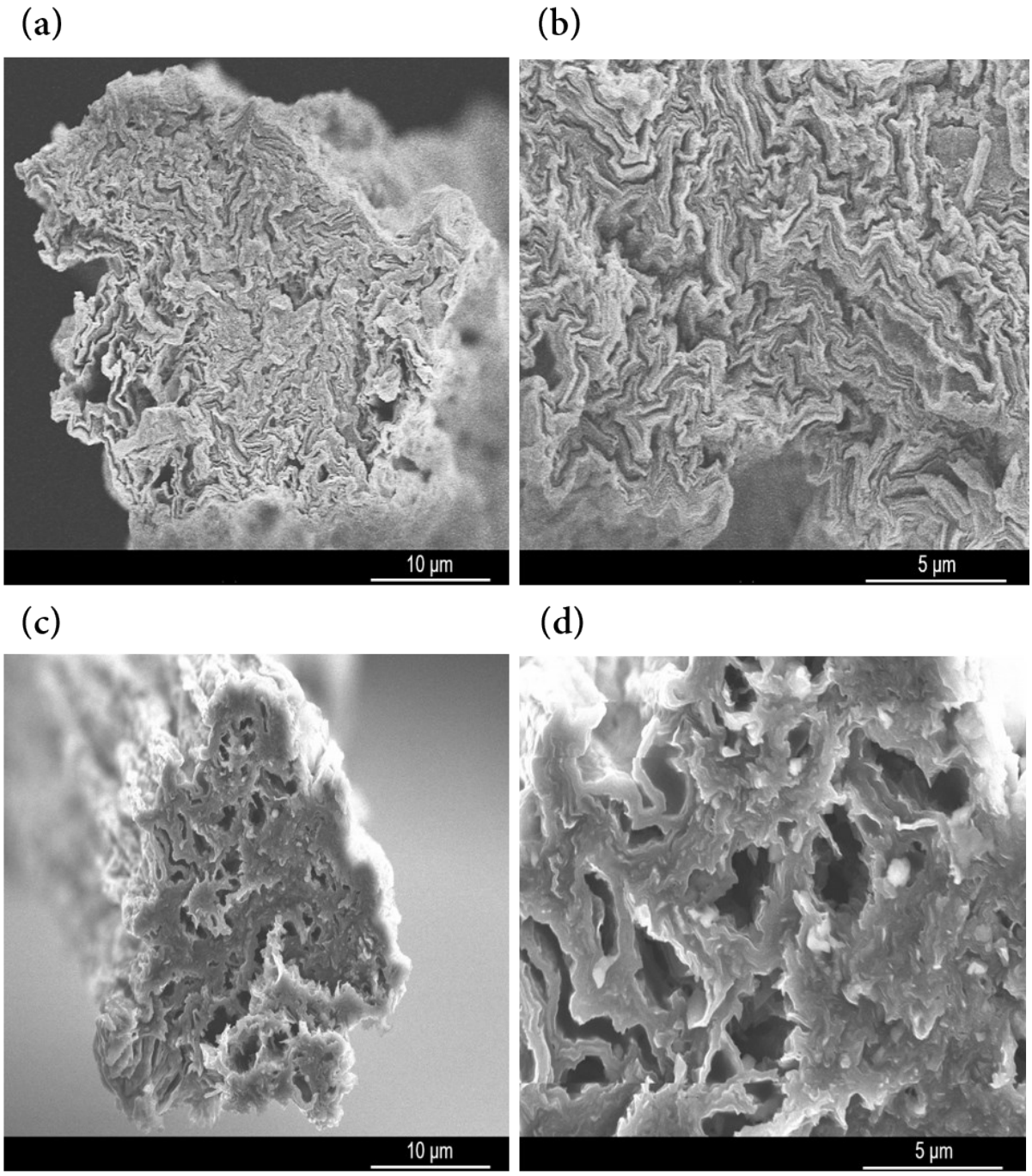

Figure S8. (a-b) Cross-sectional SEM image of wet-spun Graphene Oxide Fiber (GOF). (c-d) Cross-sectional SEM image of thermally reduced Graphene Oxide Fiber (rGOF) at 700°C.

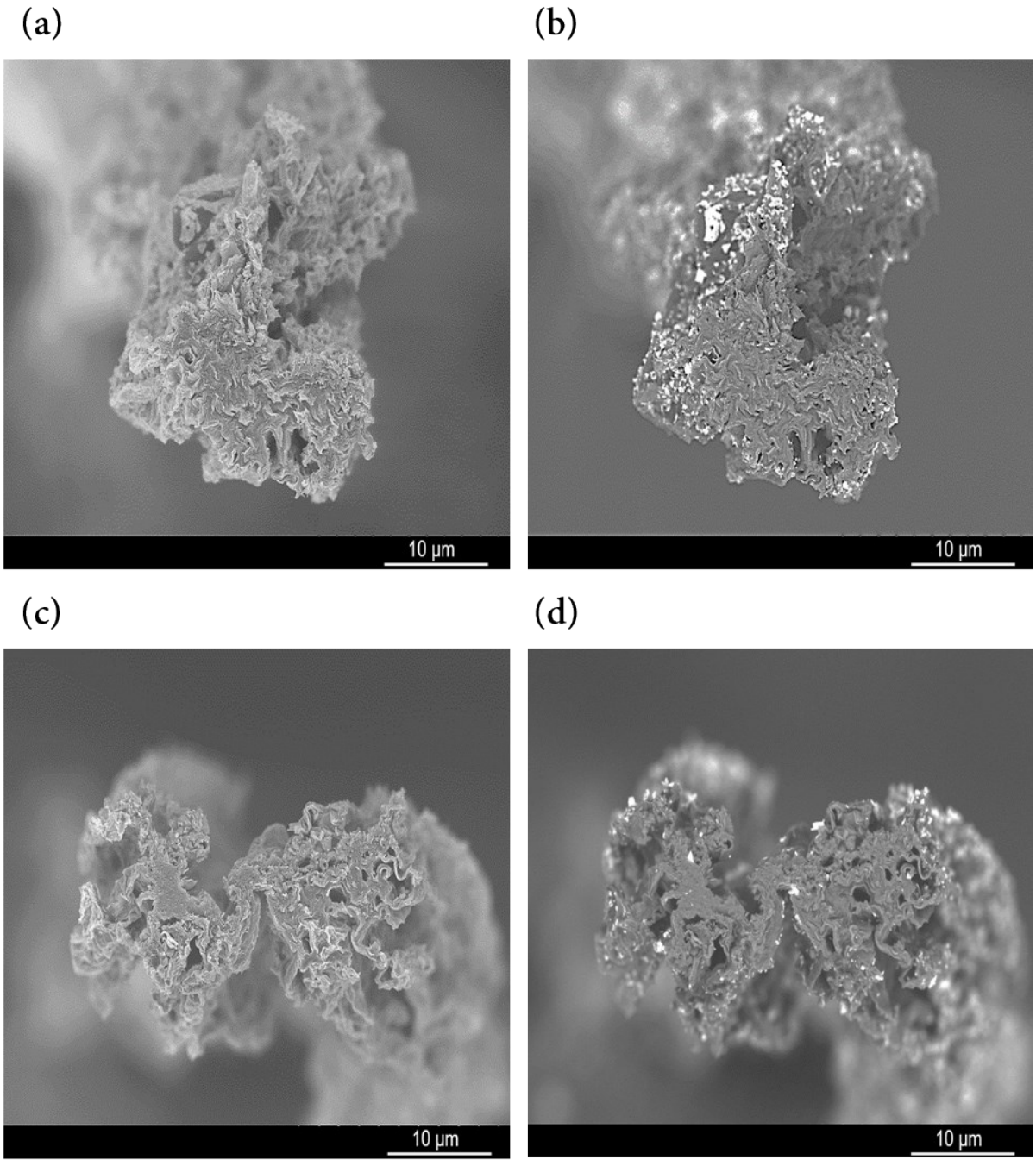

Figure S9. (a) Cross-sectional SEM image of WO_3-rGO fiber (b) The corresponding BSE image. (c) Cross-sectional SEM image of WN-rGO fiber (d) The corresponding BSE image.
BSE images show the outward attachment of active materials as a result of the hydrothermal process.

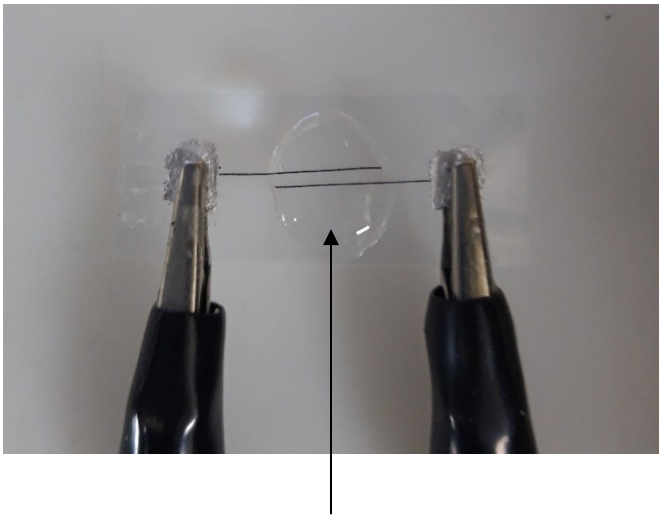

Figure S10. Photograph showing the formation of fiber supercapacitor devices used for electrochemical analysis. This setup is referred to as 2-electrode parallel configuration.

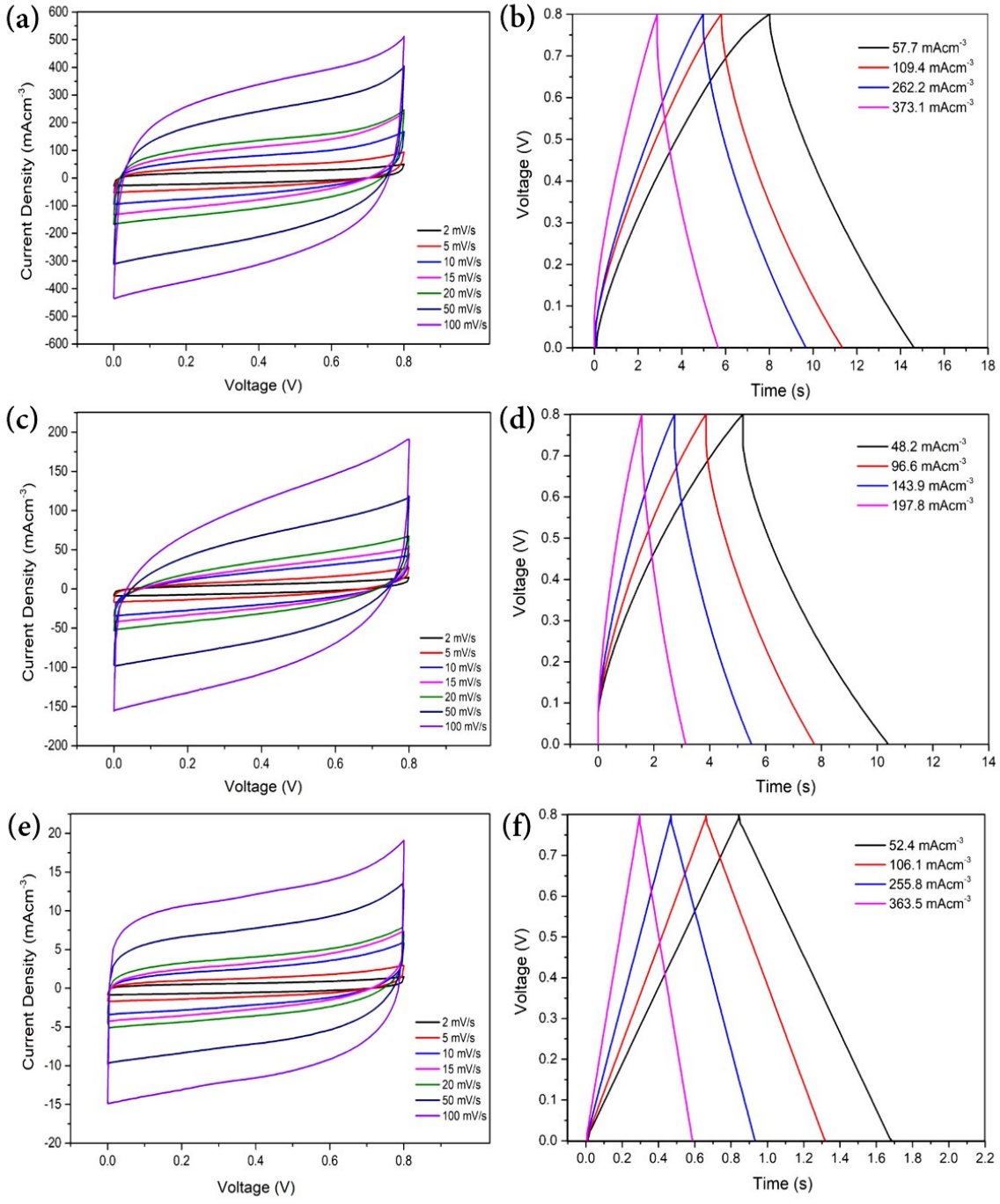

Figure S11. (a, c, e) CV curves of WN-rGOF, WO_3-rGOF and rGOF supercapacitors respectively at different scan rates. (b, d, f) GCD plots of WN-rGOF, WO_3-rGOF and rGOF supercapacitors respectively at different current densities.

Fiber	Current Density (A/cm^3)	Capacitance (F/cm^3)	Energy Density (mWh/cm^3)	Discharge time (s)	Power Density (W/cm^3)
rGOF	0.0524	2.16	0.192	0.83	0.832
	0.1061	1.91	0.169	0.65	0.936
	0.2558	1.56	0.1386	0.46	1.084
	0.3635	1.12	0.0995	0.29	1.235
		Retention = 51.8 %	**Retention = 51.8 %**		
WO_3-rGOF	0.0482	9.31	0.8275	5.4	0.551
	0.0966	8.44	0.7502	4.1	0.658
	0.1439	6.19	0.5502	2.9	0.683
	0.2478	4.05	0.3601	1.8	0.72
		Retention = 43.5 %	**Retention = 43.5 %**		
WN-rGOF	0.0577	16.29	1.448	6.7	0.778
	0.1094	14.75	1.311	5.6	0.842
	0.2622	11.4	1.013	4.1	0.889
	0.3731	7.49	0.6657	2.6	0.921
		Retention = 46.0 %	**Retention = 46.0 %**		

Table S2. Electrochemical performance values of fibers at different Current Densities.

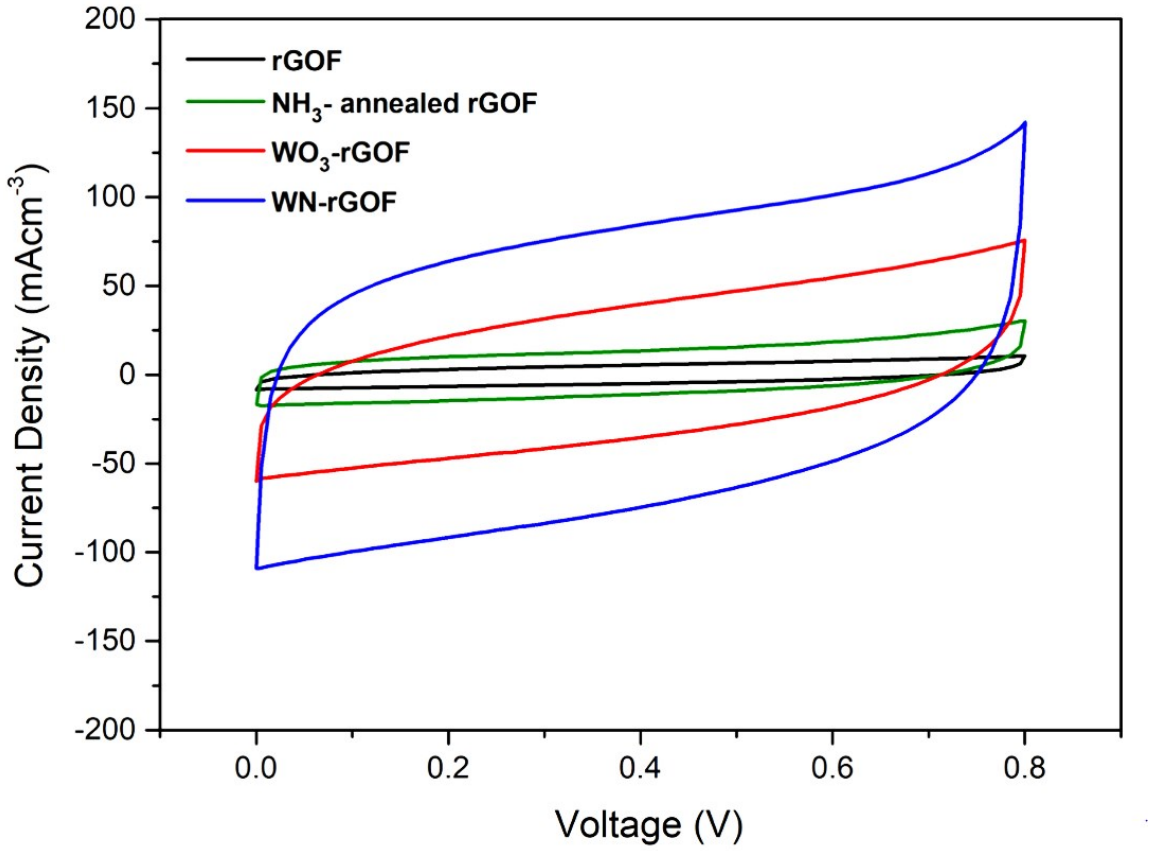

Figure S12. Cyclic voltammetry curve comparison of NH_3-annealed rGOF supercapacitor with the rest of the fiber supercapacitors at 10 mV/s.

Supplementary Note 1. Determination of optimized mass loading of WN in WN-rGOF.

The electrochemical characteristics of WN-rGOF with different WN loading were examined by controlling the concentration of the precursor material $Na_2WO_4.2H_2O$ in order to identify the fiber with the optimized WN content. The concentration of precursor for WN-rGOF is labelled as "x", and the fibers with varied concentrations are named according to their concentration difference relative to "x" as described in Table S3. Figure S13 (a-e) shows the morphology of WN-rGOF at different concentrations. As seen in the SEM images, the amount of WN present on the fiber varies according to the concentration used. As expected, the capacitance of WN-rGOF keeps rising with the quantity of WN as seen in Table S2 and the area of CV curves in Fig S13 (f). However, this rise becomes less significant when the concentrations reach 3 times and 4 times the original concentration. This is because at such high concentrations, the active material fully covers or overgrows the surface of the fiber as evident from the SEM images. As the contact between the active material and the fiber would keep declining, such high concentrations would only hinder electrolyte penetration. Therefore, it becomes equally important to look at the capacitance retention instead of solely focusing on the capacitance values. Figure S14 (a-e) shows the CV curves of WN-rGOF with different concentrations from 10-100 mV/s. A capacitance retention plot in terms of scan rate is plotted in Fig S14 (f) based on these CV curves and the values are listed in Table S3. It can be seen that WN-rGOF-4, WN-rGOF-3 and even WN-rGOF-2 exhibit worse capacitance retention compared to WN-rGOF. On the other hand, although WN-rGOF-0.5 presents a slightly better retention, it possesses a much lower capacitance due to insufficient WN. On this basis, WN-rGOF, having 23.81 wt.% of WN, can be identified to have the optimum combination of capacitance and capacitance retention as shown in Figure S15.

The weight of the fibers was measured using an ultra-sensitive Mettler Toledo XPE 26 Balance. The wt.% of WN in each fiber was found by weighing the hybrid fibers of equal length (i.e. 5 cm) and comparing it to the weight of 5 cm long rGO fiber as shown in the table.

Fiber name	Concentration of Precursor = x (mmol/liter)	Weight of fiber (mg)	wt.% of WN	Capacitance of FSC (F/cm^3)	Capacitance retention (%)
WN-rGOF-0.5	0.5 x = 1.75 mmol	0.024	14.28 %	11.63	47.12 %
WN-rGOF	**x = 3.5 mmol**	**0.026**	**23.81 %**	**16.14**	**45.78 %**
WN-rGOF-2	2 x = 7 mmol	0.029	38.09 %	22.15	29.82 %
WN-rGOF-3	3 x = 10.5 mmol	0.033	57.14 %	25.76	19.56 %
WN-rGOF-4	4 x = 14 mmol	0.038	80.95 %	28.24	14.80 %

* Length of the fibers = 5 cm

* Weight of rGOF (5 cm length) = 0.021 mg

Table S3. Electrochemical performance of WN-rGOF at different wt.% of WN.

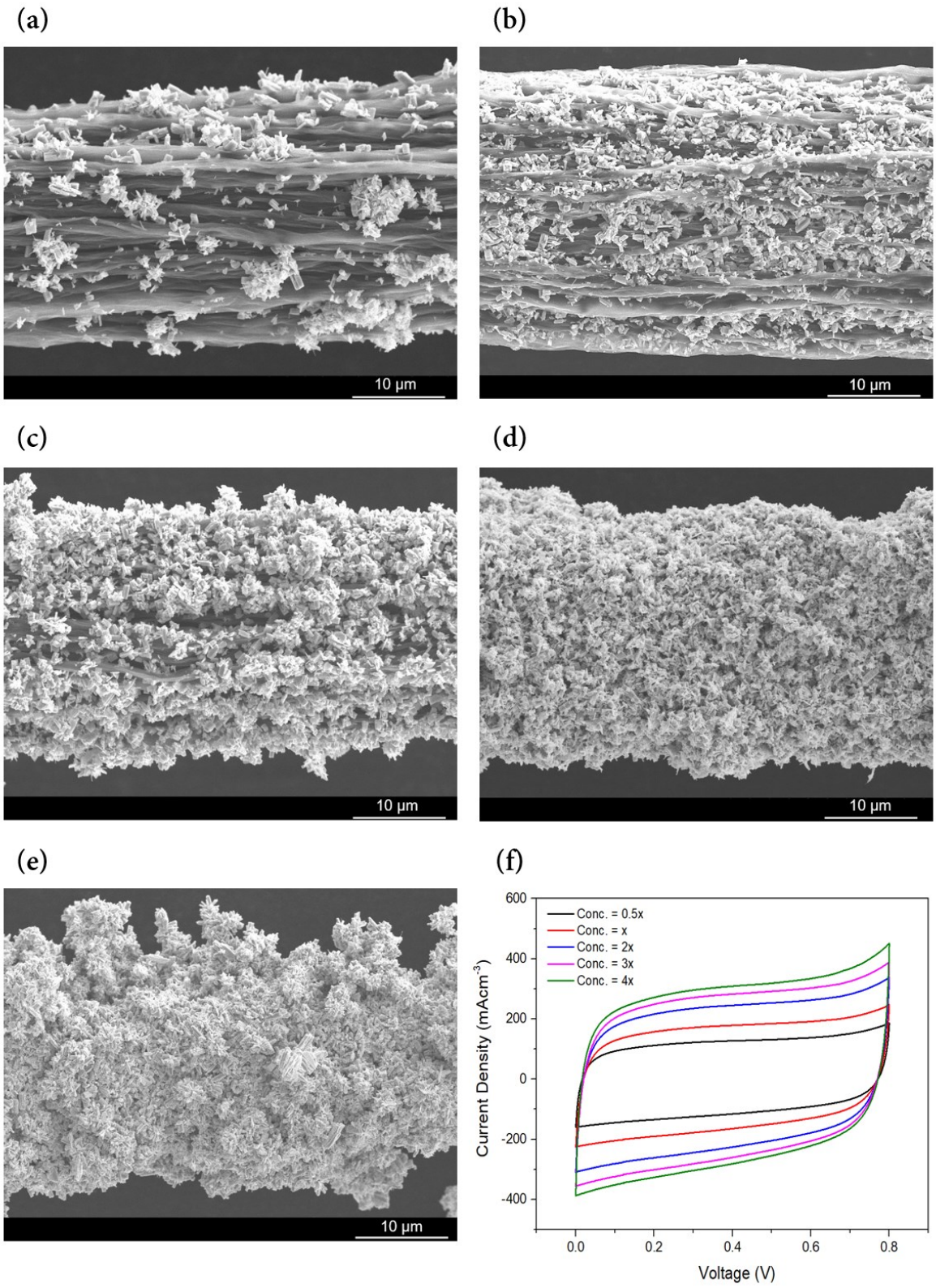

Figure S13. (a-e) Lateral SEM images of WN-rGOF at different precursor concentration of WN. (a) WN-rGOF-0.5 (b) WN-rGOF (c) WN-rGOF-2 (d) WN-rGOF-3 (e) WN-rGOF-4 (f) CV curves of WN-rGOF with different precursor concentration of WN at 10 mV/s.

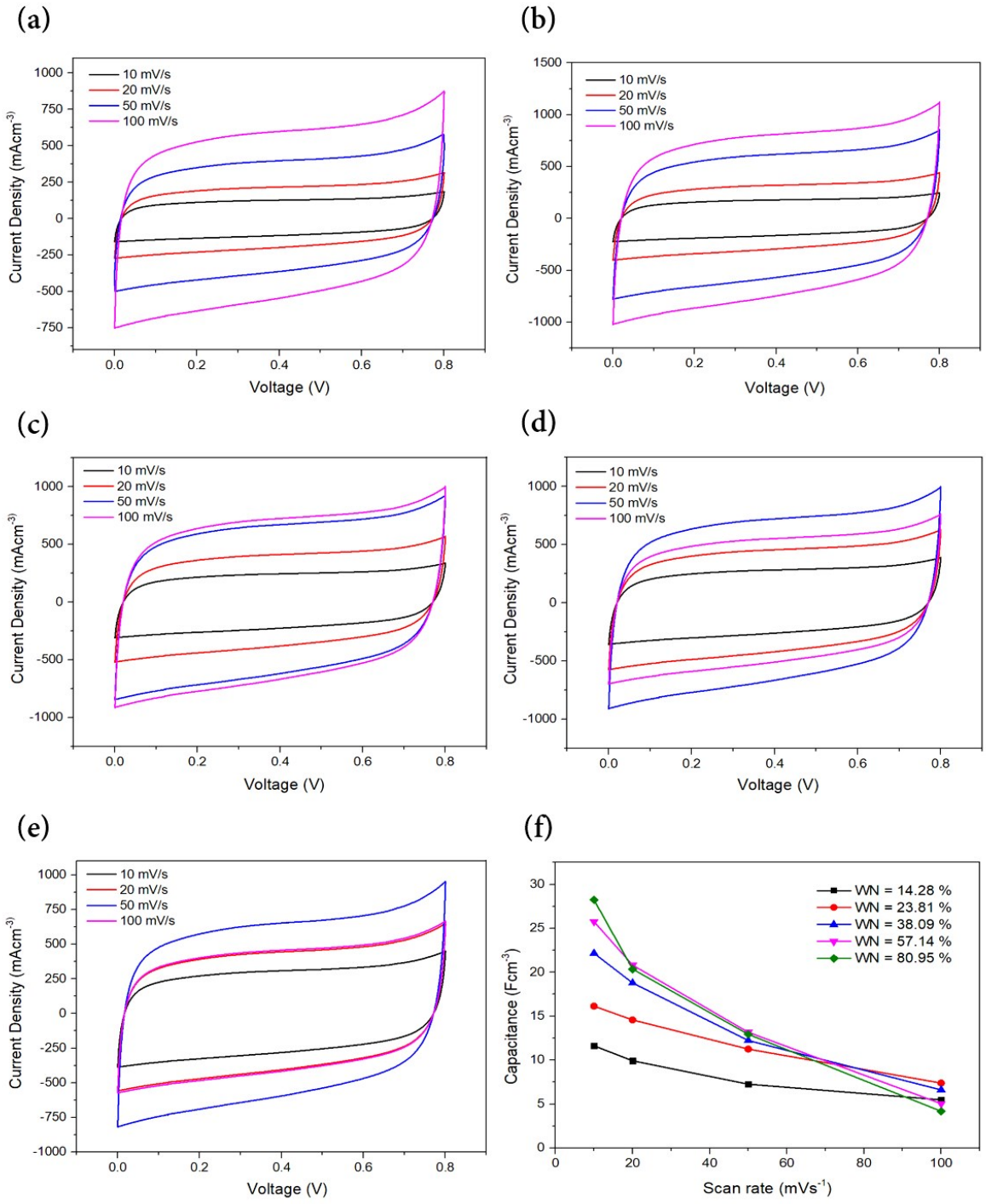

Figure S14. (a-e) CV curves of WN-rGOF with different precursor concentration of WN at scan rates of 10-100 mV/s. (a) WN-rGOF-0.5 (b) WN-rGOF (c) WN-rGOF-2 (d) WN-rGOF-3 (e) WN-rGOF-4 (f) Capacitance retention plot of WN-rGOF with different wt.% of WN.

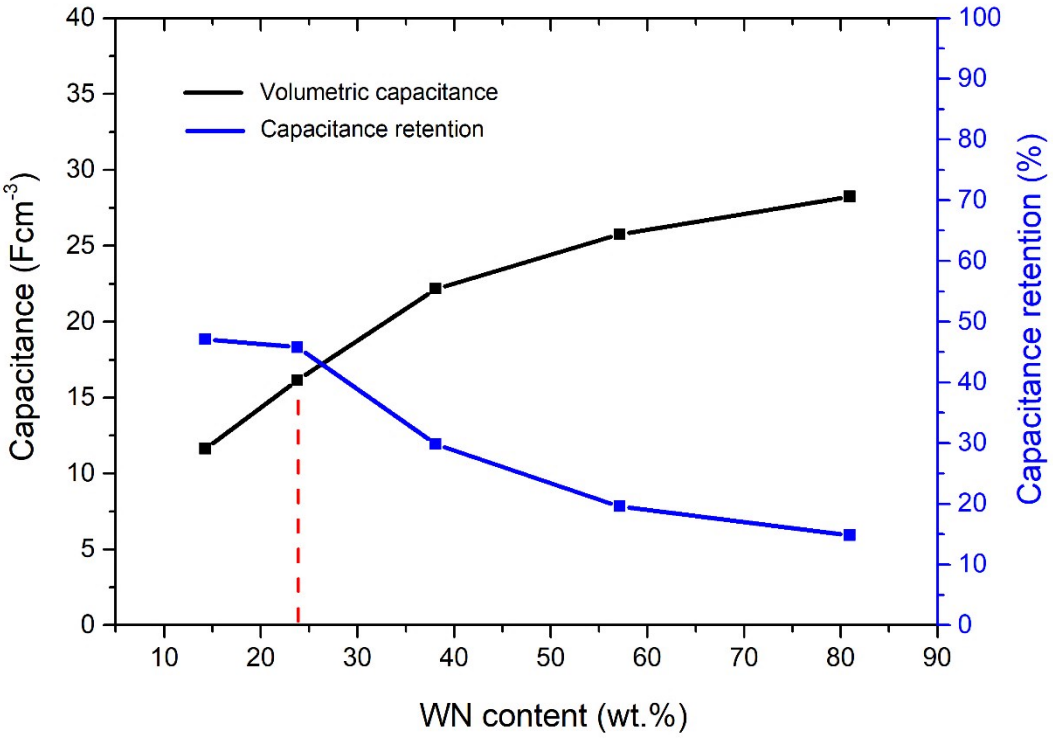

Figure S15. Variation of Volumetric Capacitance and Capacitance Retention of WN-rGO fibers with different mass loadings of WN.

Supplementary Note 2. **Calculation of Q_{total}, Q_s and Q_d.**

The total amount of charge stored is calculated from the CV curves using the equation:

$$Q_{total} = \int I \, . \, dt = I \frac{dV}{v} = \frac{Area\ under\ the\ curve}{Scan\ rate} \quad (15)$$

Here, $Q_{total} = Q_s + Q_d$ (16)

According to the model $i=av^b$, the capacitive charge Q_s is independent of scan rate (for low scan rates such as 2-20 mV/s). However, the diffusion-controlled charge Q_d keeps decreasing by increasing scan rate, due to which total charge also gets reduced with increasing scan rate [S1].

The value of Q_s can be found from the plot of Q_{total} vs scan rate$^{-1/2}$ by linear fitting and subsequent extrapolation to y-axis as shown in Fig. 4b. The equation in Fig. 4b shows the linear fitting to find the intercept value Q_s. The y-intercept gives the value of Q_s. Q_d can then be calculated by subtracting Q_s from Q_{total} as described in Table S4.

Scan rate (mVs^{-1})	Scan rate $^{-1/2}$ ($mV^{-1/2}s^{1/2}$)	Q_{total} (C/cm^3)	Q_s (C/cm^3)	Q_d (C/cm^3)
2	0.707	54.3	30.573	23.727
5	0.447	46.4	30.573	15.827
10	0.316	41.8	30.573	11.227
15	0.258	38.9	30.573	8.327
20	0.224	37.9	30.573	7.327

Table S4. The values of Q_{total}, Q_s and Q_d at the mentioned scan rates.

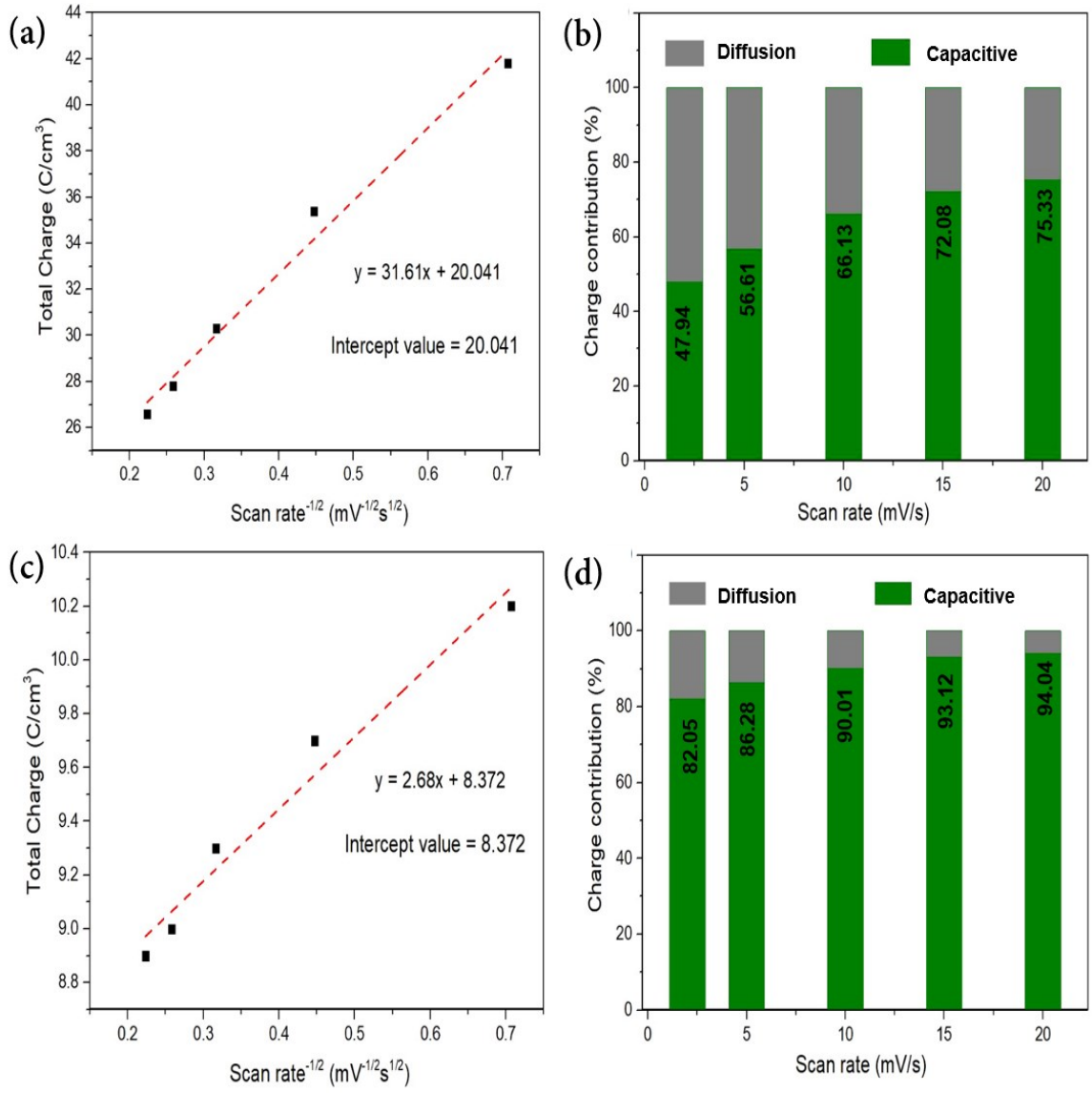

Figure S16. (a) Total amount of charge stored in WO_3-rGOF at scan rates of 2, 5, 10, 15, and 20 mV/s. (b) Percentage of surface capacitive and diffusion-controlled charge contributions in WO_3-rGOF at the aforementioned scan rates. (c) Total amount of charge stored in rGOF at scan rates of 2, 5, 10, 15, and 20 mV/s. (d) Percentage of surface capacitive and diffusion-controlled charge contributions in rGOF at the aforementioned scan rates.

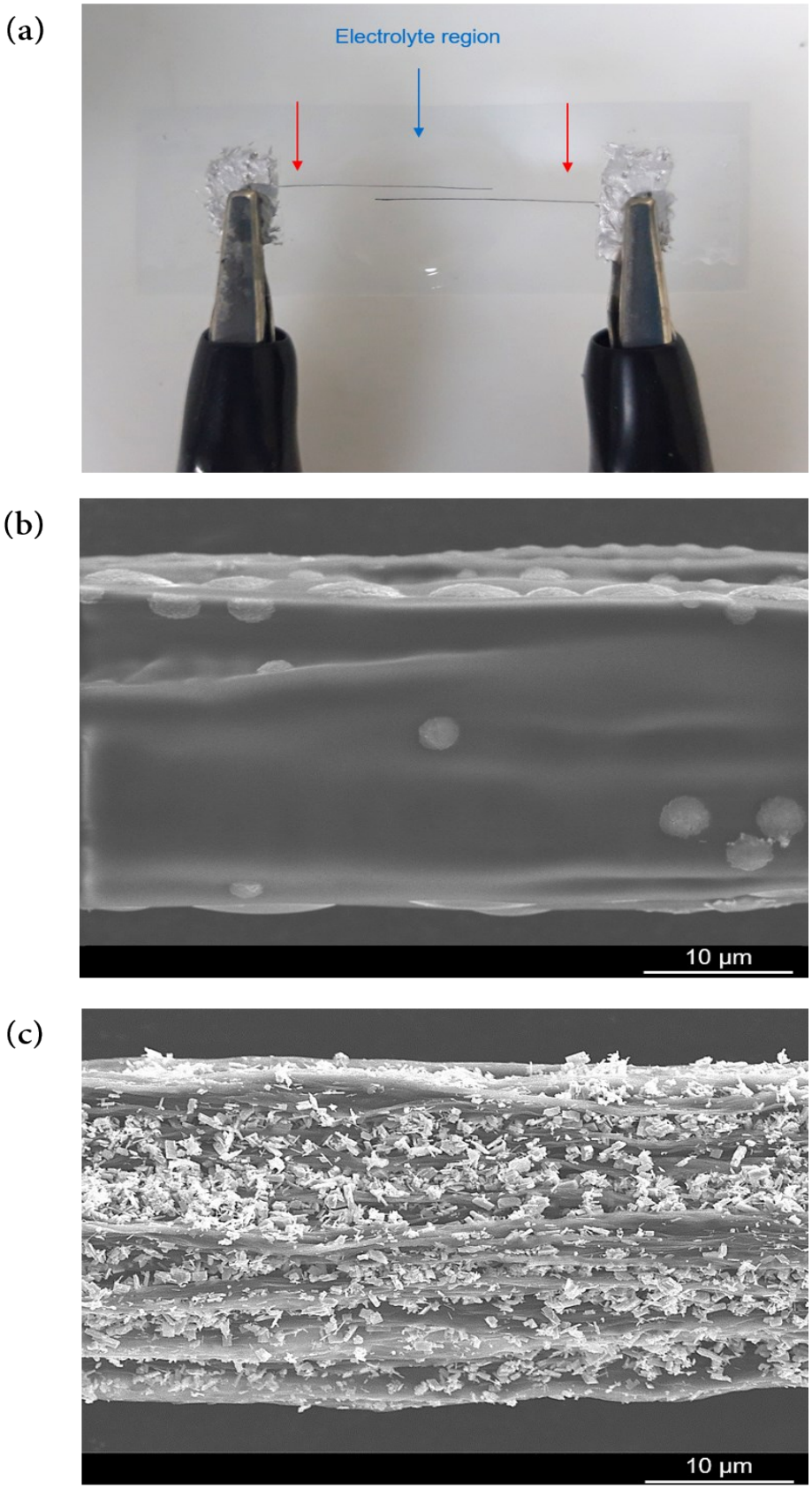

Figure S17. (a) Photograph of WN-rGOF supercapacitor after the cycle test. Regions marked in red represent the area of fiber outside the electrolyte. (b) SEM image of WN-rGOF inside the electrolyte region, marked by blue. (c) SEM image of WN-rGOF outside the electrolyte region, marked by red.

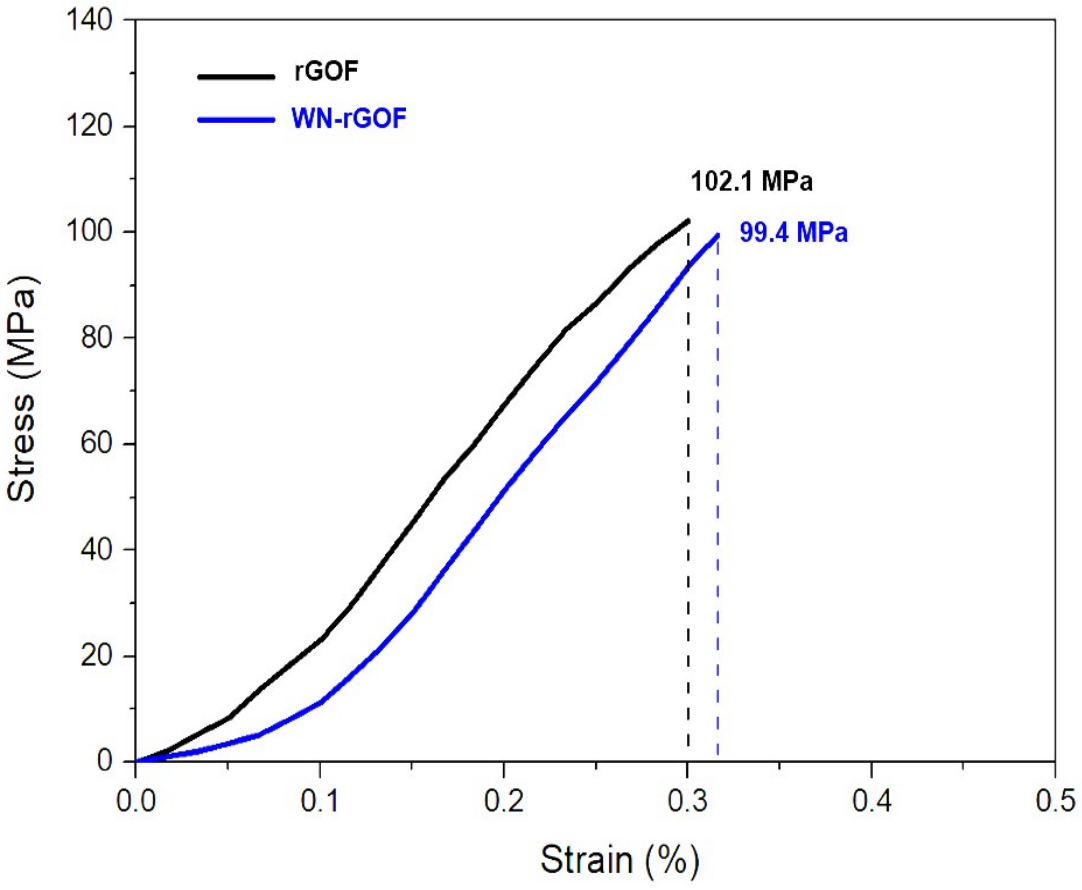

Figure S18. Stress-strain curves for rGOF and WN-rGOF.

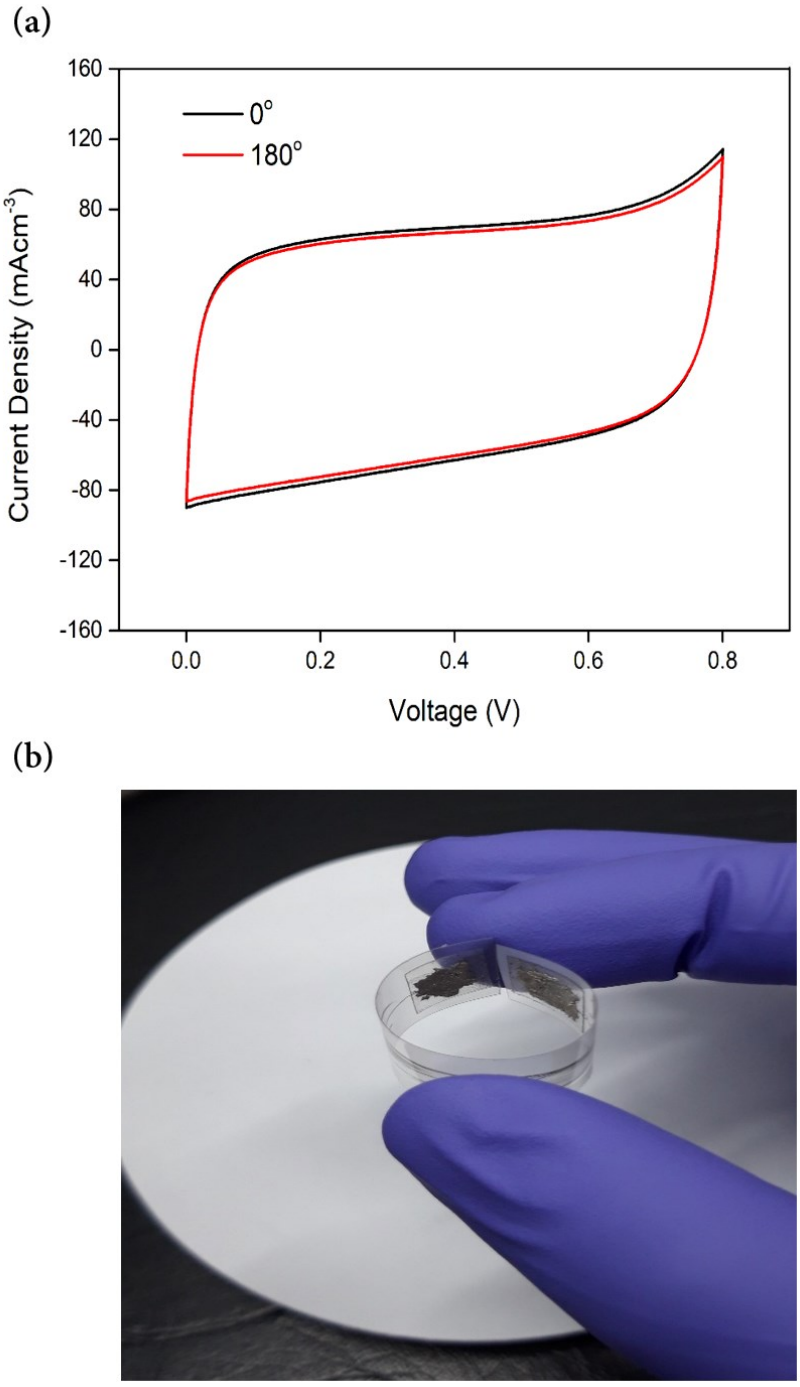

Figure S19 (a). CV curve comparison of WN-rGOF supercapacitor under normal and 180° bending state. **(b)** Demonstration of flexibility of WN-rGOF supercapacitor under 360° folding.

Supplementary Note 3. Three-electrode cell test.

The three electrode cell tests were conducted by making a cell in which the fibers or the nanocubes were utilized as the working electrode, a Platinum wire as the counter electrode, and Ag/AgCl (3M KCl) as the reference electrode. The electrolyte used for the electrochemical measurements was 1M H_2SO_4.

The volumetric and gravimetric capacitance values from three electrode tests were calculated by their CV curves using the following equations respectively.

$$C_{f,\,vol} = \frac{1}{2vV\Delta E}\int IdE \tag{17}$$

$$C_{f,\,grav} = \frac{1}{2vm\Delta E}\int IdE \tag{18}$$

where v is the scan rate, E is the voltage window, V is the volume of the fiber and m is the mass of the fiber.

Figure S19 (a) shows the CV curves of WO_3 and WN nanocubes obtained using a three-electrode cell configuration in 1M H_2SO_4 electrolyte. The redox peaks appearing in the CV curves of the nanocubes can be attributed to the following reactions respectively.

$$\mathbf{WO_3 + xH^+ + xe^- \longleftrightarrow HWO_3} \tag{19}$$

$$\mathbf{WN + xH^+ + xe^- \longleftrightarrow HWN} \tag{20}$$

The electrochemical performance of individual fibers was also tested in three-electrode cell using the same 1M H_2SO_4 electrolyte. The CV curves as shown in Figure S19 (b-c) were used for the calculation of the gravimetric and volumetric capacitances of the individual fibers respectively and the values are enlisted in Table 1. The redox peaks in the hybrid fibers appear at approximately the same potentials as the individual nanocubes, indicating the presence of pseudo-capacitance. However, the peaks become considerably faint in case of hybrid fibers as the conductive fiber surface increases the speed of the reversible redox reactions to a significant extent [S2-S4].

As the surface capacitive processes comprise of EDLC and pseudocapacitance, the analysis of these contributions should also be carried out. For this purpose, the specific capacitances of rGOF and hybrid fibers are compared with the individual nanocubes.

The specific capacitance (C_{grav}) of WO_3 and WN nanocubes calculated from CV curves at $2mVs^{-1}$ are 136.7 and 167.4 F/g respectively. Meanwhile, as seen in Table 1, the hybrid fibers of WO_3-rGOF and WN-rGOF show much larger $C_{f,\ grav}$ of 206.2 and 347.7 F/g, respectively, in comparison to rGOF (28.5 F/g). It is known that the limited $C_{f,\ grav}$ of rGOF is mainly due to the presence of only EDLC mechanism [S3]. Thus, it is evident that pseudocapacitance brought by WO_3 and WN is the major contributing factor in the hybrid fibers as the $C_{f,\ grav}$ of rGOF increases sharply after the introduction of these active materials.

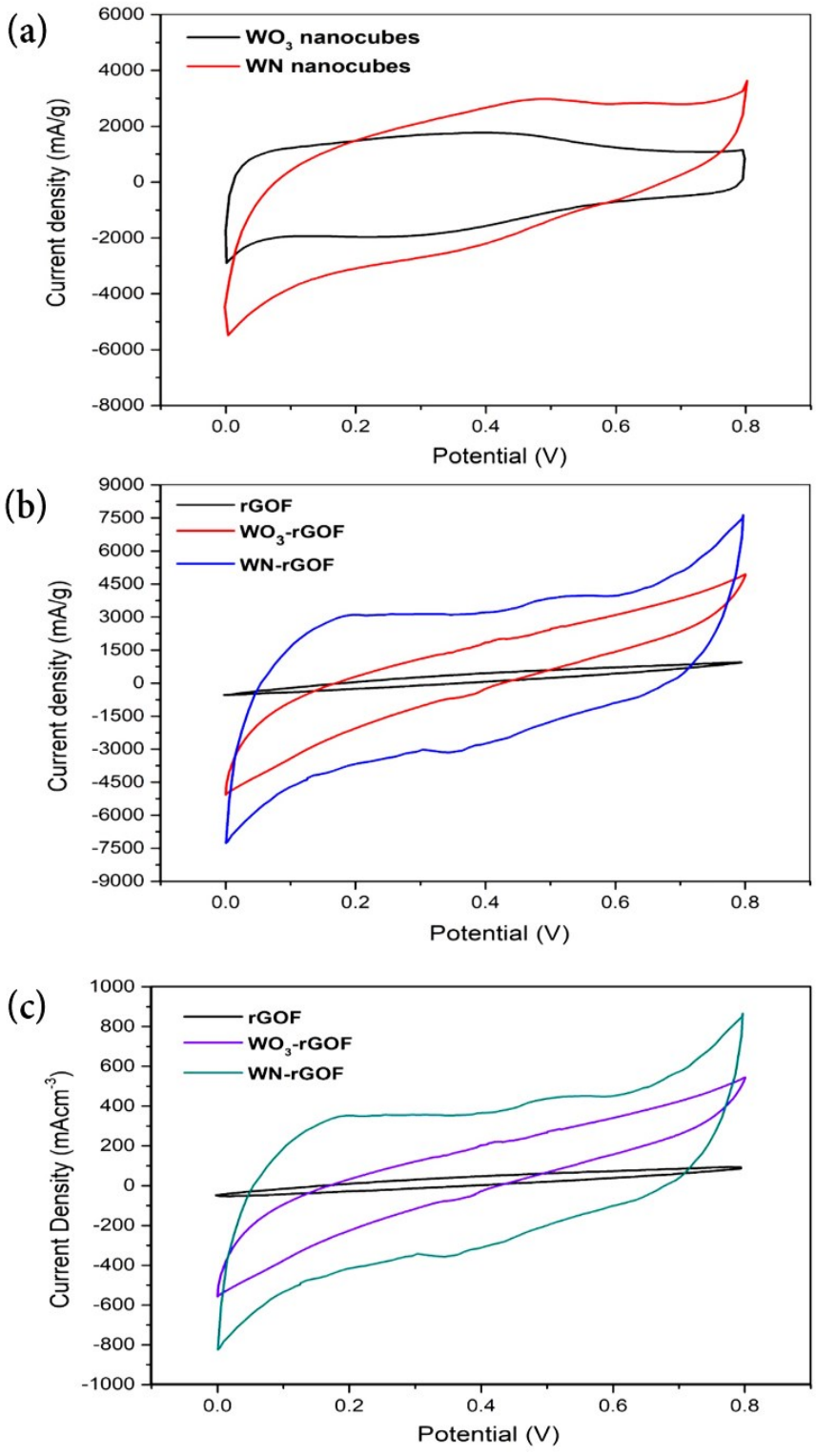

Figure S20. Three-electrode tests at 2mV/s. (a) CV curves for WO_3 and WN nanocubes used for the calculation of their gravimetric capacitance. (b) CV curves for rGOF, WO_3-rGOF and WN-rGOF used for the calculation of their gravimetric capacitance. (c) CV curves of rGOF, WO_3-rGOF and WN-rGOF used for the calculation of their volumetric capacitance.

Reference

[S1] V. Lokhande, A. Lokhande, G. Namkoong, J. H. Kim and T. Ji, *Results in Physics,* 2019, **12**, 2012-2020.

[S2] S. P. Sasikala*,* K. E. Lee, J. Lim, H. J. Lee, S. H. Koo, I. H. Kim, H. J. Jung and S. O. Kim, *ACS Nano,* 2017*,* **11**, 9424-9434.

[S3] S. Zhai*,* C. Wang, H. E. Karahan, Y. Wang, X. Chen, X. Sui, Q. Huang, X. Liao, X. Wang and Y. Chen, *Small,* 2018, **14**, 1800582.

[S4] F. Z. Amir, V. H. Pham, D. W. Mullinax and J. H. Dickerson, *Carbon*, 2016, **107**, 338-343.